resistance at finite temperatures. Because such a probability decreases with temperature, the fluctuation supercurrent, and hence the conductance, increases. Zero resistance is reached only at $T = 0$ K.

Note added in proof: After the submission of this manuscript, superconductivity in ropes of nanotubes was reported (*28*).

References and Notes

1. D. Jerome, A. Mazaud, M. Ribault, K. Bechgaard, *J. Phys. (Paris) Lett.* **41**, L95 (1980).
2. T. Ishiguro, K. Yamaji, G. Saito, *Organic Superconductors* (Springer, Berlin, ed. 2, 1998).
3. A. F. Hebard *et al.*, *Nature* **350**, 600 (1991).
4. K. Tanigaki *et al.*, *Nature* **352**, 222 (1991).
5. J. H. Schon, Ch. Kloc, B. Batlogg, *Nature* **408**, 549 (2000).
6. A. Yu. Kasumov *et al.*, *Science* **284**, 1508 (1999).
7. The possibility of superconductivity in carbon nanotubes has been predicted, with a transition temperature that increases with decreasing diameter owing to the enhanced electron-phonon interaction. See (*29*).
8. Z. K. Tang, H. D. Sun, J. N. Wang, J. Chen, G. D. Li, *Appl. Phys. Lett.* **73**, 2287 (1998).
9. N. Wang, Z. K. Tang, G. D. Li, J. S. Chen, *Nature* **408**, 50 (2000).
10. P. Launois *et al.*, *Solid State Commun.* **116** (2), 99 (2000).
11. H. D. Sun, Z. K. Tang, J. Chen, G. D. Li, *Appl. Phys.* A **69**, 381 (1999).
12. Magnetic and electrical transport measurements were reproducible on the same sample over a period of a few months, indicating that the nanotubes inside the AFI channels were stable.
13. There is some evidence that at very small magnetic fields there is a difference between the field-cooled and zero-field–cooled data. However, the measured magnetization signals are too small to be definitive. At 0.2 T, the measured magnetization is substantially above the noise level.
14. The anisotropy in the measured magnetic data suggests that the data are unlikely to arise from random magnetic impurities, because such an effect should be isotropic with respect to the field orientation.
15. For an infinite tube with a radius R, the Meissner effect under a parallel field requires a circumferential surface current. However, quantization of electronic motion in the circumferential direction means that the electron energy levels are discrete, with an average level separation that varies as $1/R^2$. Thus, as R diminishes to zero, the 1D system is necessarily insulating in the transverse direction, i.e., there is no circumferential current.
16. V. L. Ginzburg, L. D. Landau, *Zh. Eksp. Teor. Fiz.* **20**, 1064 (1950).
17. P. G. de Gennes, *Superconductivity of Metals and Alloys* (Benjamin, New York, 1966), p. 171.
18. For polarization transverse to the SWNTs, the sample is transparent to visible light, whereas for polarization parallel to the SWNTs, the sample is opaque. This is an indication that the sample is insulating in the transverse direction.
19. Because the superconducting region may be as large as 50 nm (indicated by the supercurrent experiment), the charging energy is small. Thus, the quantum effect would apply only at very low temperatures.
20. N. Metropolis, A. W. Rosenbluth, M. N. Rosenbluth, A. H. Teller, E. Teller, *J. Chem. Phys.* **21**, 1087 (1953).
21. K. Binder, Ed., *Monte Carlo Methods in Statistical Physics* (Springer-Verlag, Berlin, 1979), p. 1. The calculations are carried out by starting at $T = 30$ K with an initial Gaussian wavefunction whose width is proportional to $1/B$. Simulated annealing is then carried out by cooling at 0.04 K intervals, and at each temperature, 10^7 to 10^8 Metropolis steps were carried out. At each Metropolis step, a random complex number ($\rho \cos\theta$, $\rho \sin\theta$) was generated, with $0 < \rho \leq 1$ and $-\pi > \theta \leq \pi$, as a potential additive change to $\psi(x)$. Spatial discretization is at the level of 16 points per coherence length, and 6 points were used to calculate the numerical derivative to third-order accuracy. The length of the sample used is $60\xi_o$ to $250\xi_o$. Down to $T \approx 0.1$ K, the finite size effect is within the statistical fluctuations of the calculated results. Meissner effect calculations were carried out by considering a 4 Å strip. Hence, in Eq. 1 the $\psi(x)$ is replaced by $\psi(x,y)$.
22. The temperature and magnetic-field variations of the magnetic susceptibility represent a reasonably constraining set of conditions for the determination of the parameter values. For example, α_o enters in both the temperature and magnetic-field variations, and $\alpha_o T_c^o$ is the energy unit in the GL theory. The error in the parameter values is estimated to be $\sim \pm 10\%$.
23. We have carried out LDA calculations on the (5,0), (3,3), and (4,2) nanotubes. Diameters are found to be 4.04, 4.20, and 4.27 Å, respectively. (4,2) is a semiconductor, whereas (5,0) and (3,3) are metallic, and the density of states at the Fermi level is 0.21 and 0.06 states per eV per C atom, respectively. The effective band mass of (3,3) is at least one order of magnitude larger than that for the (5,0). The metallicity of (5,0) is due to strong σ-π mixing induced by the large curvature of the tube. Large-scale LDA calculation has also been carried out in regard to the Peierls transition in the nanotubes. The negative results indicate that the transition temperature could be very low.
24. It also implies weak interaction between the nanotubes and the walls of the zeolite channels, because with a zeolite thickness of only 7.4 Å between the nanotubes, any interaction between the nanotubes and the zeolite channel walls would translate into interaction between the nanotubes.
25. Z. K. Tang, H. D. Sun, J. N. Wang, *Physica* B **279**, 200 (2000).
26. By estimating the average superconducting segment as 0.1-μm long and taking the low-temperature intercept as 4 V, our sample (with a thickness of 100 μm) has about 1000 superconducting segments, separated by potential barriers. That translates into a measured low-temperature gap width of ~4 meV, which is in good agreement with the BCS formula of $2\Delta(0) = 3.6kT_c^o \approx 4$ meV.
27. ΔG increases with temperature for $T > 15$ K. Such nonmetallic behavior is not unusual for a 1D Luttinger liquid.
28. M. Kociak *et al.*, *Phys. Rev. Lett.* **86**, 2416 (2001).
29. L. X. Benedict, V. H. Crespi, S. G. Louie, M. L. Cohen, *Phys. Rev.* B **52**, 14935 (1995).

30. We thank K. Y. Lai for technical assistance with the FIB system and T. K. Ng, P. Yu, and L. Chang for helpful comments. Partially supported by University Grants Committee of Hong Kong grants HIA98/99.SC01 and DAG 00/01.SC27, Research Grants Council grant HKUST 6152/99P, and SAE Company grant SAE 95/96.SC01.

7 March 2001; accepted 17 May 2001

Construction Principles of "Hyparenes": Families of Molecules with Planar Pentacoordinate Carbons

Zhi-Xiang Wang* and Paul von Ragué Schleyer†

Density-functional theory calculations predict that three borocarbon units with planar pentacoordinate carbons $-C_3B_3-$, $-C_2B_4-$, and $-CB_5-$, can replace the $-(CH)_3-$ subunits in aromatic or even in antiaromatic hydrocarbons to construct "hyparenes" (families of molecules with planar pentacoordinate carbons). These borocarbon units contribute two, one, and zero electrons, respectively, to the parent pi system. Depending on the choice of these units, the hyparenes (judging from computed proton and nucleus-independent chemical shifts), can maintain or can interconvert the aromatic or antiaromatic character of the parent compounds. The hyparenes are low-lying local minima with normal carbon-boron, boron-boron, and carbon-carbon bond lengths. The multicenter bonding in the hyparenes involves contributions of partial sigma and partial pi bonds to the planar pentacoordinate carbons; the octet rule is not violated. Borocarbon species, for which there is some mass spectrometric evidence, might be observed and identified, for example, in matrix isolation by vibrational spectroscopy.

The principles of the mechanical molecular models for hydrocarbons, still widely used to visualize organic structures, have remained essentially unchanged since van't Hoff introduced folded paper tetrahedra (*1*, *2*) as the first three-dimensional representation. Placed corner-to-corner, two of these methane tetrahedra represent ethane. Two tetrahedra joined edge-to-edge have four coplanar vertices and model ethylene. Similarly, an acetylene model results from a face-to-face arrangement.

Here we predict simple structural groupings, based on planar pentacoordinate carbons (ppC) [$-C_3B_3-$ (type **A**), $-C_2B_4-$ (type **B**), and $-CB_5-$ (type **C**)] (Fig. 1),

Center for Computational Quantum Chemistry, Computational Chemistry Annex, University of Georgia, Athens, GA 30602–2525, USA.

*Permanent address: Graduate School at Beijing, University of Science and Technology of China, Academia, Sinica, Beijing 10039, People's Republic of China.

†To whom correspondence should be addressed. E-mail: schleyer@chem.uga.edu

which are fundamentally different from the traditional trigonal sp^2 arrangements. We show how **A**, **B**, and **C** can function as building blocks to construct the simple molecules (**1**, **2**, and **3**) and elaborate numerous aromatic and antiaromatic hydrocarbons to give "hyparenes" (hypercoordinated arenes) including **4**, **5**, and **6** (Fig. 1) and **7** through **19** (Fig. 2) [more examples are given in Web fig. 1 (*3*)]. All these species have computed structures (*4*) with normal bond lengths (*5*), vibrational spectra with no imaginary frequencies, and magnetic properties [nucleus-independent chemical shifts (NICS) (*6*) as well as proton chemical shifts] that reveal the aromatic or antiaromatic character of the individual rings (Table 1) (*7*). The planar pentacoordination results from multicenter bonding. However, the total Wiberg bond indices (WBI) for the central carbons range from 3.65 to 3.95 (Table 1) and show that the octet rule is not violated (*8*).

The demonstration that molecules with a planar hexacoordinate carbon, such as **20** (Fig. 3), can be viable (*9*) led us to explore higher degrees of planar hypercoordination computationally (*10*). The D_{7h} geometry of CB_7^-, **21** (with a planar heptacoordinate carbon) is a minimum, but the D_{8h} geometry of CB_8 (with carbon in the center) has two imaginary frequencies (*11*). The carbon atom is too small to achieve good bonding to all eight boron atoms simultaneously and moves to a ring edge upon further optimization in lower symmetry. The resulting minimum, **22**, features a ppC. No prior ppC example has been described, to our knowledge, even though "hypercarbons" with three-dimensional carbon pentacoordination are quite common (*12*).

As in **20** and **21**, six π electrons are involved in **22**. Moreover, **22** contains a unit of type **C**. Replacement of the three dicoordinate borons in **22** by three CH groups gives **6** (also with six π electrons), in which the

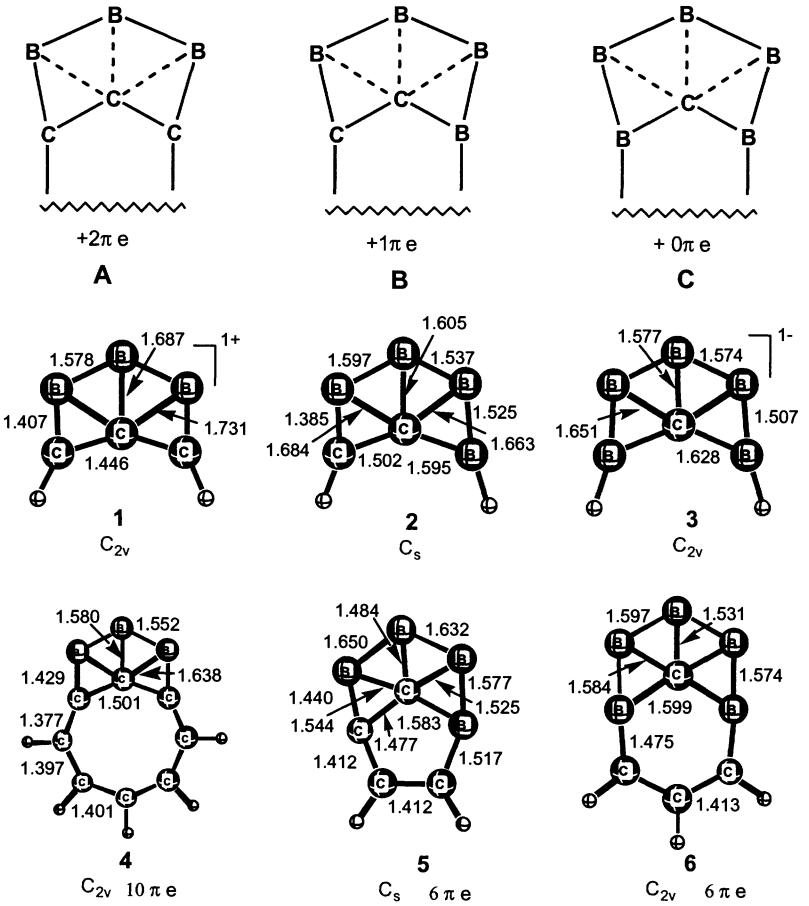

Fig. 1. Conceptual relation of the building units **A**, **B**, and **C** to stable isoelectronic 4π species with planar pentacoordinate carbons (**1** to **3**) and the hyparenes **4**, **5**, and **6**.

Table 1. Theoretical results for the hyparenes **4** to **19** and **22**. For compounds with two entries, the first refers to the ring (or carbon) shown on the left in Fig. 2, and the second to the right. ν_1 is the smallest vibrational frequency at B3LYP/6-31G*. Tot. π e, total π electron occupancies given by NBO analysis. $\Delta\pi$, number of π electrons contributed by **A** through **C**. δH, average H chemical shifts at GIAO-B3LYP/6-311+G**//B3LYP/6-311+G**. As references, the average δH values for aromatic benzene, naphthalene, and azulene (both rings) are 7.6, 7.9, and 8.0 ppm, respectively, whereas those for antiaromatic cyclobutadiene and benzocyclobutadiene are 4.8 and 6.6 (four-ring) and 6.1 (six-ring), respectively. NICS(1), values at GIAO-B3LYP/6-311+G**//B3LYP/6-311+G**. For reference, the NICS(1) for aromatic benzene, naphthalene, and azulene are −10.2, −10.6, and −7.8 (seven-membered ring) and −17.8 (five-membered ring), respectively, whereas the NICS(1) for the antiaromatic cyclobutadiene, pentalene, and benzocyclobutadiene are 17.5, 18.2, and 13.4 (four-ring) and −2.8 (six-ring), respectively. Tot. ppC WBI, total Wiberg Bond Index for the ppCs at B3LYP/6-31G*//B3LYP/6-31G*.

Hyparene	ν_1	Tot. π e	$\Delta\pi$	δH	NICS(1)	Tot. ppC WBI
4	155.1	9.97	1.82	7.7	−12.9	3.94
5	111.1	5.98	1.03	8.1	−9.9	3.78
6	163.8	5.98	0.1	8.6	−8.8	3.70
7	102.9	9.97	1.73	7.4	−14.4	3.89
8	115.2	11.94	1.89	5.2, 3.2	0.6, 18.5	3.91
9	156.4	9.94	1.97		−13.1	3.93
10	65.2	9.99	1.01	8.8	−10.4	3.86
11	119.5	7.97	1.02	2.0	30.9	3.83
12	96.4	9.96	0.98	9.2	−10.5	3.86
13	71.4	12.04	0.98	0.7	24.8	3.81
14	118.4	7.97	0.19	7.0, 6.1	14.7, −3.3	3.71
15	95.7	9.98	0.17	8.5, 8.4	10.2, −8.3	3.70
16	63.0	7.84	0.11	5.4	9.2	3.73
17	140.3	9.96	1.78, 1.17	8.2	−10.7	3.83, 3.72
18	94.5	9.99	1.78, 0.20	8.8	−9.7	3.95, 3.76
19	54.9	9.97	0.94, 0.21	9.3	−2.9, −12.5	3.82, 3.65
22	134.8	5.98			−24.0	3.91

five borons bind the central carbon more effectively than in **22**. Note that **6** can be regarded as benzene extended by a type **C** unit. That the $4n + 2$ aromaticity rule is followed is confirmed by the negative NICS(1) (*13*) and downfield H nuclear magnetic resonance (NMR) chemical shifts (δH) (*14*).

Most mono- and polycyclic aromatic (and even antiaromatic) species (referred to here generically as "arenes") can be extended geometrically and electronically by the borocarbon groups **A** to **C**. Appropriately chosen, these extensions either can maintain existing aromaticity (for example **C** in **6**) or can convert antiaromatic into aromatic systems (for example **A** in **4**) and vice versa. Group **A** simply replaces three adjacent hydrogens of an allyl or of an arene–$(CH)_3$–fragment by three borons. This increases the total electron count by six. These extra electrons can be assigned (with some oversimplification) as follows: two electrons help form a fourth (for example B-B) σ bond (in addition to the three CH bonds of the original species), two electrons are involved in four-center–two-electron (4c-2e) bonding of the central carbon with three borons (shown by the dashed lines in **A** to **C**), and two electrons from **A** add to the existing π electron count. Group **B** not only replaces three hydrogens, but also one carbon atom by boron; a second carbon-boron replacement characterizes **C**. Hence, **B** adds one π electron, whereas **C** does not change the π electron count. Simple isoelectronic molecules illustrate these groups: neutral $C_2B_4H_2$ (**2**) belongs to group **B**, the $CB_5H_2^-$ anion (**3**) to group **C**, and the $C_3B_3H_2^+$ cation (**1**) to group **A** (Fig. 1). Note that **1**, **2**, and **3** all have four π electrons, but exhibit the diatropic ring currents associated with aromaticity. Because deltahedral multicenter bonding (*15*), both σ and π, is involved in **1**, **2**, and **3**, the CC, CB, and BB bonds have normal lengths.

Unit **A**, acting as a two π electron donor, converts the antiaromatic tub-shaped cyclooctatetraene into a planar aromatic 10 π electron system (**4**). Similarly, the antiaromatic pentalene becomes aromatic **7** after incorporation of an **A** unit (Fig. 2). The average proton chemical shifts, δH, of **4** and **7** (Table 1) are in the region for typical aromatic compounds. Attached once to naphthalene, group

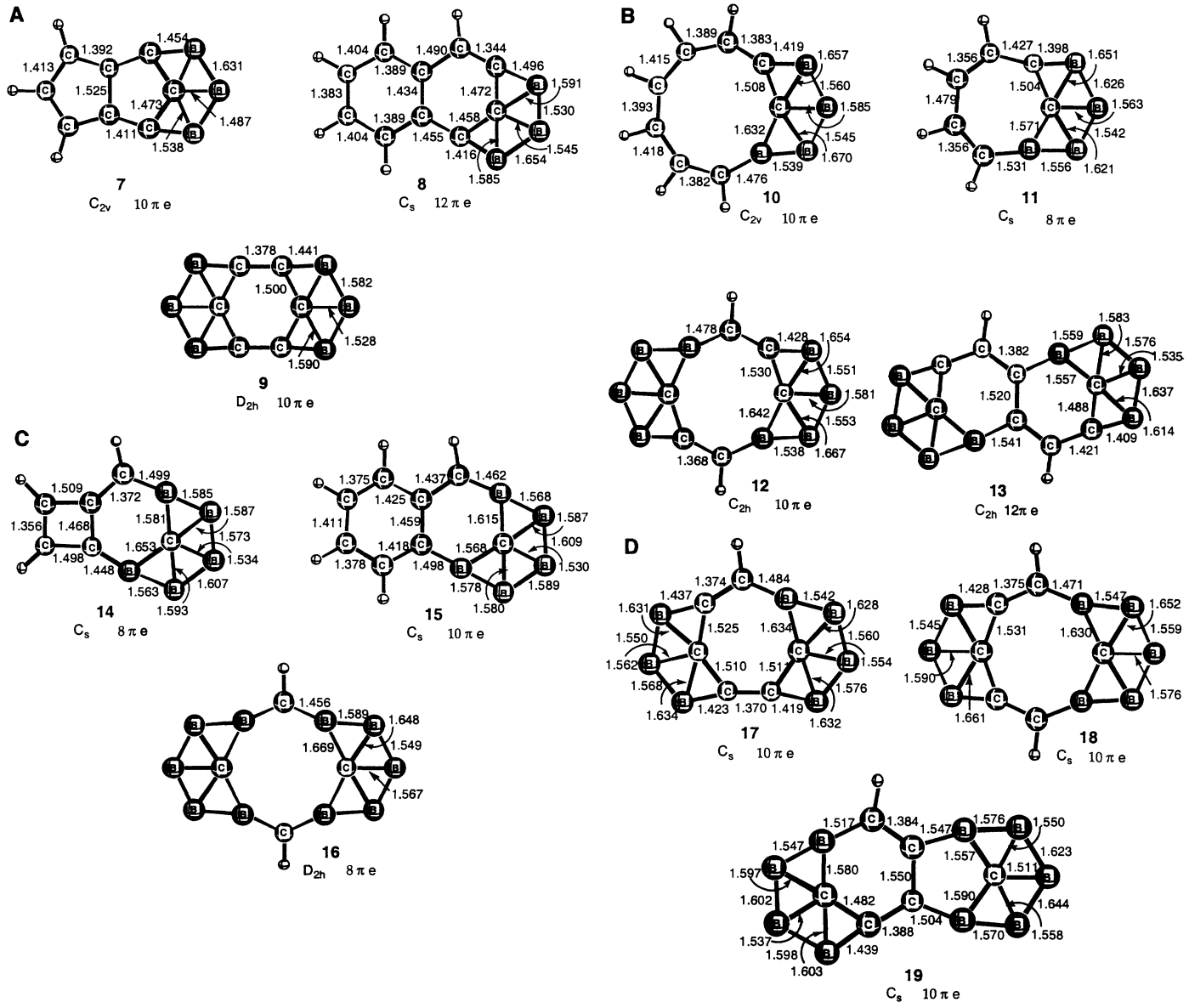

Fig. 2. Examples of hyparenes incorporating type **A** (**7** to **9**) (**A**); **B** (**10** to **13**) (**B**); **C** (**14** to **16**) (**C**); and mixed **A**, **B**, and **C** (**17** to **19**) (**D**) units. More examples are given in Web fig. 1 (*3*).

A results in an antiaromatic, albeit still planar, molecule, **8**, with 12 π electrons. Attached twice to benzene (thereby replacing all the protons and adding four π electrons), **A** gives the borocarbon, C_6B_6 (**9**), which is an aromatic 10 π electron system. Unlike all other species reported in this paper, the planar benzene with one **A** unit had an instable wavefunction.

Aromatic neutral hyparenes with singlet ground states are predicted by using **B**, which contributes one π electron, to extend $4n + 1$ π electron annulene systems. Thus, cyclopentadienyl ($n = 1$) gives **5** and cyclononatetraenyl ($n = 2$) gives **10** (Fig. 2); the latter has a 10 π electron aromatic planar nine-membered ring. Conversely, unit **B** renders $(CH)_x$ ($x = 4n + 3$, $n = 1, 2\ldots$) systems antiaromatic. An example is **11**, which has strong bond length alternation, positive NICS(1) (+30.9), and a strongly upfield δH of 2.0. Two **B** units contribute a total of two π electrons and invert the aromaticity (or antiaromaticity) of an arene. Thus, the doubly substituted cyclooctatetraene (**12**) is aromatic, whereas the doubly substituted naphthalene (**13**) is antiaromatic.

Unit **C** adds no extra π electrons and does not alter the existing aromaticity (or antiaromaticity). In addition to **6**, we have elaborated a host of polycyclic aromatic hydrocarbons by one or more **C** units (Fig. 2). The singly substituted benzocyclobutadiene (**14**) retains its antiaromaticity, whereas **15** retains the aromaticity of its parent (naphthalene). Despite being antiaromatic, the doubly substituted cyclooctatetraene **16** also has a planar eight-membered ring. This illustrates the "robustness" as well as the rigidity of the **A**, **B**, and **C** "construction units" and their inherent planarizing abilities, even in the absence of aromaticity.

Units **A**, **B**, and **C** also can be combined, as exemplified by **17** to **19** (Fig. 2). The expected 10 π electron count is consistent with the NICS(1) and H chemical shifts (Table 1). Combinations of **A**, **B**, and **C** can also create antiaromatic hyparenes [see Web fig. 1 (*3*)].

To be observable as isolated species (e.g., in the gas phase or in matrix isolation), these predicted hyparene minima should be stable toward dissociation and should have relatively large barriers toward rearrangements. Due to its relation to benzene, **9** (C_6B_6) was chosen for detailed exploration. Remarkably, the atomization energy (1390.7 kcal/mol) of **9** is larger than that (1289.3 kcal/mol, both computed at B3LYP/6-311+G**) of benzene. The strength of the deltahedral bonding in the ppC structures also is reflected by the rather normal BB and BC bond lengths (*5*) and by their wide adaptability not only to aromatic but also to antiaromatic hyparenes. The high rigidity of the aromatic C_6 ring strongly hinders the rearrangement of **9** into the isomers without C_6 rings. Structural isomers with C_6 rings are much less stable than **9**: the only minimum (**23**) (Fig. 4) we have found is 136.4 kcal/mol higher in energy than **9**. However, some structurally more remote isomers (i.e., without C_6 rings) [see Web fig. 3 (*3*)] are lower in energy than **9**. The vertical ionization energy of **9** (7.8 eV), comparable with 7.5 eV for azulene and 8.0 eV for naphthalene, also implies its stability.

Although boron carbide is a familiar material, very little is known about binary boron-carbon (borocarbon) compounds. The laser ablation study of Becker and Dietze (*16*) recorded the mass spectra of a great number of binary boron-carbon anions and cations ($B_nC_m^{+\text{ or }-}$) (including $C_6B_6^+$), but no structural information is available. Clearly, experiments should be directed at generating, separating, isolating, and identifying (e.g., by vibrational spectroscopy) (*17*) individual borocarbons. Even those without ppCs can be expected to have unusual structures (*18*, *19*).

Although no examples have been identified experimentally as yet, the hyparenes are unusual in combining planar hypercoordinate carbon and aromaticity. They extend our knowledge of chemical bonding and promise to enrich and to bridge organic and inorganic chemistry. The unusual structures of the hyparenes may confer special properties useful for the design of new materials. The recent exciting discovery (*20*) that magnesium diboride (MgB_2) exhibits superconductivity (T_c = 39 K) further stimulates interest in borocarbons with their unusual electronic structures. Our computational results challenge preparative chemists. The examples presented here deliberately focused on carbon as the "central" atom and are only illustrative. Analogs with planar pentacoordinate borons (or other elements) are equally viable; isomers of **1** to **19** with hypercoordinate central borons (instead of carbon) can be lower in energy (e.g., **24** and **25** in Fig. 4 are 23.6 and 44.9 kcal/mol more stable than **9**). Note that **24** contains a ppC and a planar pentacoordinate boron. Outer rings involving atoms other than boron and carbon in perimeters are possible (*21*). Units **A** through **C** may be expected to have counterparts containing transition metal (*22–24*) groups. Initial results show that construction units similar to **A** through **C** but based on planar tetracoordinate carbon also are possible (*25*). A potentially rich hypercoordinate "flat carbon chemistry" can be foreseen.

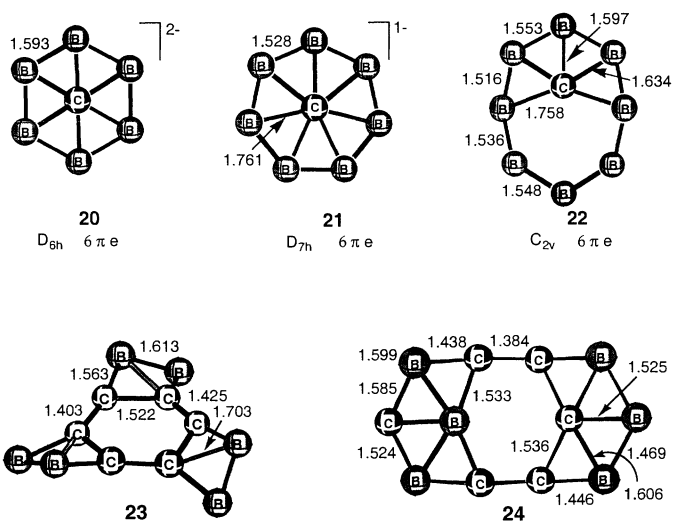

Fig. 3. Minima with planar hexacoordinate (**20**), heptacoordinate (**21**), and pentacoordinate (**22**) carbons. The latter was optimized by following one of the degenerate imaginary frequencies of the octacoordinate CB_8 (D_{8h}) structure.

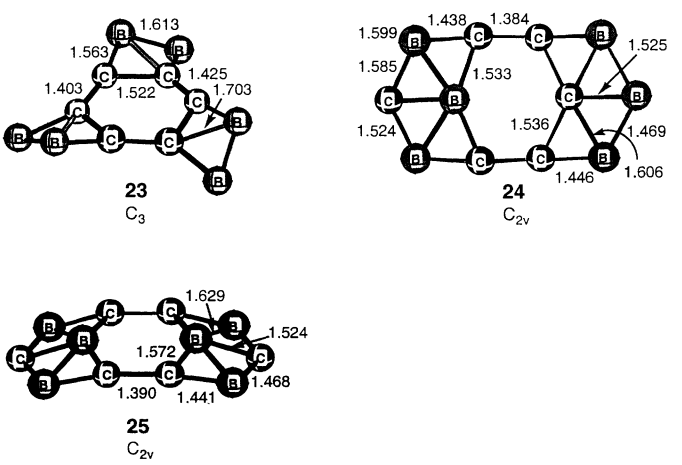

Fig. 4. Representative C_6B_6 isomers of **9**.

Reference and Notes

1. J. H. van't Hoff, *Arch. Neerl. Sci. Exactes Nat.* 445 (1874). For a reproduction of this paper, see http://dbhs.wvusd.k12.ca.us/Chem-History/Van't-Hoff-1874.html
2. For J. H. van't Hoff's booklet, *The Arrangement of Atoms in Space*, see www.chem.yale.edu/~chem125/125/history/vanthoff/tetrahedra.html
3. Web figures 1 through 4 and table 1 are available at *Science* Online at www.sciencemag.org/cgi/content/full/292/5526/2465/DC1.
4. All structures were first optimized at B3LYP/6-31G* and were shown to be minima by frequency calculations and to have stable wavefunctions, The geome-

tries then were refined at B3LYP/6-311+G**. Correlated ab initio methods (CCSD(T)/6-311+G** for **1** to **3**, MP2/6-31G* and MP2/6-311+G** for **1** to **6**) were employed to reoptimize some of the geometries as further checks. Frequency calculations at MP2/6-311+G** for **1** to **3** and MP2/6-31G* for **1** to **6** further confirm they are minima [Web fig. 2 (3)]. All calculations were carried out using Gaussian G98 (M. J. Frisch *et al.*, Gaussian, Pittsburgh, PA, 1998).
5. Typical reference bond length at B3LYP/6-311+G** are: r_{CC} = 1.531 Å in ethane, 1.396 Å in benzene, and 1.329 Å in ethene; r_{CB} = 1.554 Å in CH_3BH_2 and 1.396 Å in CH_2BH; and r_{BB} = 1.629 Å in D_{2d} H_2BBH_2.
6. P. v. R. Schleyer *et al.*, *J. Am. Chem. Soc.* **118**, 6317 (1996). An extended bibliography of NICS is given by S. Patchkovskii and W. Thiel [*J. Mol. Model.* **6**, 67 (2000)].
7. The data in Table 1 confirm (i) the expected π electron counts (π_{tot}) from natural bond orbital (NBO) analysis [A. E. Reed, L. A. Curtiss, F. Weinhold, *Chem. Rev.* **88**, 899 (1988)]; (ii) that the π occupancy increments ($\Delta\pi$) contributed by **A**, **B**, and **C** are close to two, one, and zero electrons, respectively; (iii) that the NICS(1) values are consistent with the Hückel rule [compounds with $4n + 2$ π electrons have negative NICS(1), whereas those with $4n$ π electrons have positive values]; and (iv) the H chemical shifts in aromatic compounds are deshielded [δHs > 7.0 parts per million (ppm)], whereas those in antiaromatic compounds are shielded (δHs < 7.0 ppm).
8. The WBI is a measure of the bond order based on natural bond orbital analysis. The individual indices for each of the five bonds to the central carbons varies, but the total WBIs to the ppCs for **4**, **5**, and **6**, as well as other hyparenes, **7** and **8** are close to 4 (Table 1).
9. K. Exner, P. v. R. Schleyer, *Science* **290**, 1937 (2000).
10. Planar tetracoordinate carbon is increasingly well represented. For the latest examples and literature references, see Z.-X. Wang, P. v. R. Schleyer, *J. Am. Chem. Soc.* **123**, 994 (2001); Z.-X. Wang *et al.*, *Org. Lett.* **3**, 9 (2001).
11. SiB_8 (D_{8h}) with a planar silicon, as well as B_9^- (D_{8h}) and CB_8 (C_{2v}) with a boron in the center are minima.
12. G. A. Olah *et al.*, *Hypercarbon Chemistry* (John Wiley, & Sons, New York, 1987).
13. NICS(1) describes the NICS value 1 Å above a ring center, where the π ring current effects dominate over the local σ contributions [P. v. R. Schleyer *et al.*, *J. Am. Chem. Soc.* **119**, 12669 (1997)].
14. In the following discussion, the NICS(1) and proton chemical shifts (δH), shown in Table 1, are used as criteria to judge aromaticity and antiaromaticity.
15. P. v. R. Schleyer, K. Najafian, *Inorg. Chem.* **37**, 3455 (1998), and references therein.
16. S. Becker, H.-J. Dietze, *Int. J. Mass Spectrom. Ion Processes* **82**, 287 (1988).
17. Computed vibrational spectra and NMR chemical shifts can be obtained from the authors on request. We will gladly cooperate with experimentalists.
18. F. M. Ge *et al*, *Chem. J. Chinese Univ.* **17**, 1458 (2001).
19. F. M. Ge *et al.*, *Chem. J. Chinese Univ.* **18**, 1838 (2001).
20. J. Nagamatsu *et al.*, *Nature* **410**, 63 (2001).
21. The D_{5h} CSi_5^{2-} dianion and its isoelectronic analogs, C_{2v} CSi_4P^- and C_{2v} CSi_3P_2, are minima with ppCs at B3LYP/6-311+G**//B3LYP/6-311+G** (P. v. R. Schleyer, K. Exner, unpublished data).
22. The closest analogy is the transition metal planar tetracoordinate carbon complex [see S. L. Buchwald *et al.*, *J. Am. Chem. Soc.* **111**, 397 (1989)].
23. D. Röttger, G. Erker, *Angew. Chem. Int. Ed. Engl.* **36**, 812 (1997).
24. W. Siebert, A. Gunale, *Chem. Soc. Rev.* **28**, 367 (1999).
25. For example, replacing two $-(CH)_3-$ subunits in cyclooctatetraene by two $-C_3B_2-$ groping gives a $C_8H_2B_4$ compound with two planar tetracoordinate carbon atoms.
26. We dedicate this paper to G. A. Olah for his contributions to hypercarbon chemistry. Z.X.W. thanks R.-Z. Liu and M.-B. Huang for their encouragement.

20 February 2001; accepted 15 May 2001

Predicting the Mesophases of Copolymer-Nanoparticle Composites

Russell B. Thompson,[1] Valeriy V. Ginzburg,[1]* Mark W. Matsen,[2] Anna C. Balazs[1]†

The interactions between mesophase-forming copolymers and nanoscopic particles can lead to highly organized hybrid materials. The morphology of such composites depends not only on the characteristics of the copolymers, but also on the features of the nanoparticles. To explore this vast parameter space and predict the mesophases of the hybrids, we have developed a mean field theory for mixtures of soft, flexible chains and hard spheres. Applied to diblock-nanoparticle mixtures, the theory predicts ordered phases where particles and diblocks self-assemble into spatially periodic structures. The method can be applied to other copolymer-particle mixtures and can be used to design novel composite architectures.

Mixtures of solid nanoparticles and block copolymers can yield complex, highly ordered composites for next generation catalysts, selective membranes, and photonic band gap materials (*1–3*). The specific morphology and hence the utility of these materials depends on the copolymer architecture and on such parameters as the size and volume fraction of the particles. Here, we present a method for calculating the morphology and thermodynamic behavior of copolymer-particle mixtures without requiring a priori knowledge of the equilibrium structures. The method combines a self-consistent field theory (SCFT) for polymers and a density functional theory (DFT) for particles. The SCFT has been remarkably successful in describing the thermodynamics of pure polymer systems (*4*), whereas DFTs capture particle ordering and phase behavior in colloidal systems (*5, 6*). Applied to a diblock-particle mixture, this technique identifies new self-assembled (SA) morphologies, where both particles and polymers spontaneously order into a mesoscopically regular pattern. We thus delineate conditions where the chains drive particles to self-assemble into continuous "nanowires" or "nanosheets." The method can also be applied to composites involving other copolymer architectures (triblocks, multiblocks, combs, stars) or blends of different polymers.

Our model system consists of a mixture of molten AB diblock copolymers and solid spherical particles. All particles have the same radius R. Each diblock consists of N segments, each of a volume ρ_0^{-1}. The fraction of A segments per chain is denoted by f. The enthalpic interaction between an A segment and a B segment is described by the dimensionless Flory-Huggins parameter, χ_{AB}. As a function of ($\chi_{AB}N$) and f, a pure diblock melt can form spatially periodic microstructures with lamellar, cylindrical, spherical, or more complicated phases.

In SCF theory, many-body interactions between differing segments are replaced by the interaction of each segment with the average field created by the other segments. Here, $w_A(\mathbf{r})$ is the value at a point $\mathbf{r}$ of the mean field felt by the A segments, $w_B(\mathbf{r})$ denotes the field for B segments, and $w_p(\mathbf{r})$ represents the field for particles. Using this approach, the free energy (*7*) for our system is given by

$$F = F_e + F_d + F_p \quad (1)$$

The first term, F_e, details the enthalpic interactions in the system:

$$F_e = \frac{1}{V}\int d\mathbf{r}[\chi_{AB}N\varphi_A(\mathbf{r})\varphi_B(\mathbf{r}) + \chi_{BP}N\varphi_B(\mathbf{r})\varphi_p(\mathbf{r}) + \chi_{AP}N\varphi_A(\mathbf{r})\varphi_p(\mathbf{r})] \quad (2)$$

where V is the volume of the system, χ_{AP} and χ_{BP} are the interaction parameters between the respective segments and particles, and $\varphi_A(\mathbf{r})$, $\varphi_B(\mathbf{r})$, and $\varphi_p(\mathbf{r})$ are the dimensionless concentrations of A segments, B segments, and particles, respectively. The diblock entropic free energy F_d is adapted from (*4*):

$$F_d = (1 - \phi_p)\ln\left[\frac{V(1-\phi_p)}{Q_d}\right] - \frac{1}{V}\int d\mathbf{r}[w_A(\mathbf{r})\varphi_A(\mathbf{r}) + w_B(\mathbf{r})\varphi_B(\mathbf{r})] \quad (3)$$

where Q_d is the partition function of a single diblock subject to the fields $w_A(\mathbf{r})$ and $w_B(\mathbf{r})$. The overall volume fraction of particles is

[1]Chemical Engineering Department, University of Pittsburgh, Pittsburgh, PA 15261, USA. [2]Polymer Science Centre, University of Reading, Whiteknights, Reading RG6 6AF, UK.

*Present address: Dow Chemical Company, Building 1702, Midland, MI 48674, USA.

†To whom correspondence should be addressed. E-mail: balazs1@engrng.pitt.edu